

NUMERICAL COMPUTATIONS FOR BIFURCATIONS AND SPECTRAL STABILITY OF SOLITARY WAVES IN COUPLED NONLINEAR SCHRÖDINGER EQUATIONS

KAZUYUKI YAGASAKI AND SHOTARO YAMAZOE

ABSTRACT. We numerically study solitary waves in the coupled nonlinear Schrödinger equations. We detect pitchfork bifurcations of the *fundamental solitary wave* and compute eigenvalues and eigenfunctions of the corresponding eigenvalue problems to determine the spectral stability of solitary waves born at the pitchfork bifurcations. Our numerical results demonstrate the theoretical ones which the authors obtained recently. We also compute generalized eigenfunctions associated with the zero eigenvalue for the bifurcated solitary wave exhibiting a saddle-node bifurcation, and show that it does not change its stability type at the saddle-node bifurcation point.

1. INTRODUCTION

We consider the coupled nonlinear Schrödinger (CNLS) equations of the form

$$\begin{aligned} i\partial_t u &= -\partial_x^2 u - (|u|^2 + \beta_1 |v|^2)u, \\ i\partial_t v &= -\partial_x^2 v - (\beta_1 |u|^2 + \beta_2 |v|^2)v, \end{aligned} \quad (t, x) \in \mathbb{R} \times \mathbb{R}, \quad (1.1)$$

where $(u, v) = (u(t, x), v(t, x))$ are complex-valued unknown functions of $(t, x) \in \mathbb{R} \times \mathbb{R}$ and $\beta_1, \beta_2 \in \mathbb{R}$ are parameters. Here we are interested in the solitary wave solutions to (1.1) of the form

$$\begin{aligned} u(t, x) &= e^{i(\omega t + cx - c^2 t + \theta)} U(x - 2ct - x_0), \\ v(t, x) &= e^{i(st + cx - c^2 t + \phi)} V(x - 2ct - x_0), \end{aligned} \quad (1.2)$$

where $\omega, s > 0$, and $c, x_0, \theta, \phi \in \mathbb{R}$ are constants, such that the real-valued functions $(U, V) = (U(x), V(x))$ satisfy $U(x), V(x) \rightarrow 0$ as $x \rightarrow \pm\infty$. Henceforth, without loss of generality, we take $c, x_0, \theta, \phi = 0$ since (1.1) is invariant under the Galilean transformations

$$(u(t, x), v(t, x)) \mapsto e^{i(cx - c^2 t)} (u(t, x - 2ct), v(t, x - 2ct)), \quad c \in \mathbb{R},$$

the spatial translations

$$(u(t, x), v(t, x)) \mapsto (u(t, x - x_0), v(t, x - x_0)), \quad x_0 \in \mathbb{R},$$

and the gauge transformations

$$(u(t, x), v(t, x)) \mapsto (e^{i\theta} u(t, x), e^{i\phi} v(t, x)), \quad \theta, \phi \in \mathbb{R}.$$

Date: June 15, 2021.

2010 Mathematics Subject Classification. Primary: 34B15, 35J61; Secondary: 35Q55, 37D10.

Key words and phrases. numerical analysis, bifurcation, nonlinear Schrödinger equations, solitary wave, spectral stability.

This work was partially supported by JSPS KAKENHI Grant Number JP17H02859.

So $(U, V) = (U(x), V(x))$ solves

$$\begin{aligned} -U'' + \omega U - (U^2 + \beta_1 V^2)U &= 0, \\ -V'' + sV - (\beta_1 U^2 + \beta_2 V^2)V &= 0, \end{aligned} \tag{1.3}$$

where the prime represents the differentiation with respect to x . In particular, (1.3) allows homoclinic solutions of which one component is identically zero, e.g.,

$$(U, V) = (U_0(x), 0), \quad U_0(x) := \sqrt{2\omega} \operatorname{sech}(\sqrt{\omega}x). \tag{1.4}$$

We refer to the solitary waves corresponding to such homoclinic solutions in (1.1) as the *fundamental solitary waves*. Blázquez-Sanz and Yagasaki [2] showed that the homoclinic solution $(U_0(x), 0)$ exhibits infinitely many pitchfork bifurcations in (1.3) when β_1 is increased from zero for β_2 fixed. This result means that the fundamental solitary wave

$$(u(t, x), v(t, x)) = (e^{i\omega t}U_0(x), 0) \tag{1.5}$$

also exhibits infinitely many ones in (1.1). Here the terminology “pitchfork bifurcation” is used with caution: a pair of homoclinic solutions to (1.3), which correspond to the same family of solitary waves of the form (1.2) in (1.1), are born at the bifurcation point.

Bifurcations and stability of solitary waves in nonlinear wave equations have been widely investigated [7, 9, 16]. For CNLS equations with the cubic nonlinearity, internal oscillations and radiation dumping of the single-hump vector solitons were studied by Yang [15] and Pelinovsky and Yang [10]. For general nonlinearity cases, Yang [14] classified possible bifurcations of solitary waves, and Pelinovsky and Yang [11] determined the stability of solitary waves under some generic nondegenerate conditions. Jackson [6] also studied the stability of solitary waves from a geometric point of view. Recently, the authors [13] used the approach of [2] and developed some techniques to detect pitchfork bifurcations of the fundamental solitary wave and spectral stability of the fundamental and bifurcated solitary waves in general CNLS equations containing (1.1). A perturbation expansion of eigenvalues of the linearized operator was directly calculated under some nondegenerate conditions which are easy to verify compared to assumptions made in [11]. In particular, for (1.1), it was shown in [13] that the solitary waves born at the first bifurcation are stable but the solitary waves born at the other bifurcations are unstable while the fundamental one continues to be stable.

In this paper, we numerically detect the pitchfork bifurcations of the fundamental solitary wave (1.5) and compute eigenvalues and eigenfunctions of the corresponding eigenvalue problems to determine the spectral stability of solitary waves born at the pitchfork bifurcations in (1.1). In particular, the numerical results, some of which were also provided in [13], demonstrate the theoretical ones obtained in [13]. Moreover, one of the bifurcated solitary waves is observed to exhibit a saddle-node bifurcation. We compute generalized eigenfunctions associated with the zero eigenvalue to show that the solitary wave does not change its stability type at the saddle-node bifurcation point. Such saddle-node bifurcations with no stability switching were proven to occur in general single nonlinear Schrödinger (NLS) equations with external potentials by Yang [17] earlier. To the authors’ knowledge, such a phenomenon has not been reported for CNLS equations before. The computer tool AUTO [4] was used for carrying out necessary computations, as in similar numerical work of [12] for the single NLS equation with an external potential.

This paper is organized as follows: In Section 2 we briefly review the theoretical results of [13] on bifurcations and the stability of solitary waves in (1.1). We give numerical computations for eigenvalues and eigenfunctions in Section 3 and for generalized eigenfunctions associated with the zero eigenvalues in Section 4. Our numerical approaches, of which a general framework was given in [12] for eigenvalues and eigenfunctions, are briefly described there before the results are provided.

2. THEORETICAL RESULTS

In this section we briefly review the theoretical results of [13] on bifurcations of the fundamental solitary wave (1.5) and the stability of the fundamental and bifurcated solitary waves in the CNLS equations (1.1).

We begin with the bifurcation result. The variational equation (VE) of (1.3) around the homoclinic solution $(U, V) = (U_0(x), 0)$ is given by

$$-\delta U'' + \omega \delta U - 3U_0(x)^2 \delta U = 0, \quad -\delta V'' + s \delta V - \beta_1 U_0(x)^2 \delta V = 0. \quad (2.1)$$

We easily see that $(\delta U, \delta V) = (U_0'(x), 0)$ is a bounded solution to (2.1). We also show that (2.1) has another bounded solution $(\delta U, \delta V) = (0, V_1^{(\ell)}(x))$, which is linearly independent of $(U_0'(x), 0)$, if and only if

$$\beta_1 = \beta_1^{(\ell)} := \frac{(\sqrt{s/\omega} + \ell)(\sqrt{s/\omega} + \ell + 1)}{2}, \quad \ell \in \mathbb{Z}_{\geq 0} := \{n \in \mathbb{Z} \mid n \geq 0\}, \quad (2.2)$$

where

$$V_1^{(\ell)}(x) = \operatorname{sech}^{\sqrt{s/\omega}}(\sqrt{\omega}x) {}_2F_1\left(-\ell', \sqrt{s/\omega} + \ell' + 1/2; \sqrt{s/\omega} + 1; \operatorname{sech}^2(\sqrt{\omega}x)\right)$$

for $\ell = 2\ell', \ell' \in \mathbb{Z}_{\geq 0}$, and

$$V_1^{(\ell)}(x) = \operatorname{sech}^{\sqrt{s/\omega}}(\sqrt{\omega}x) \tanh(\sqrt{\omega}x) {}_2F_1\left(-\ell', \sqrt{s/\omega} + \ell' + 3/2; \sqrt{s/\omega} + 1; \operatorname{sech}^2(\sqrt{\omega}x)\right)$$

for $\ell = 2\ell' + 1, \ell' \in \mathbb{Z}_{\geq 0}$. Here ${}_2F_1$ denotes the hypergeometric function

$${}_2F_1\left(\begin{matrix} a, b \\ c \end{matrix}; z\right) = \sum_{j=0}^{\infty} \frac{(a)_j (b)_j}{j! (c)_j} z^j,$$

where a, b, c are constants, $(x)_j := \Gamma(x+j)/\Gamma(x)$, and $\Gamma(x)$ is the Gamma function. See Section 5 of [2] or Section 6 of [13]. The case of $\omega = 1$ was considered there by replacing ωt and s/ω with t and s , respectively, without loss of generality.

Define the integral,

$$\begin{aligned} \bar{a}_2 &= -2 \int_{-\infty}^{\infty} V_1^{(\ell)}(x)^2 \operatorname{sech}^2 x \, dx < 0, \\ \bar{b}_2 &= 8(\beta_1^{(\ell)})^2 \int_{-\infty}^{\infty} \phi_{11}(x) V_1^{(\ell)}(x)^2 \operatorname{sech} x \left(\int_x^{\infty} \phi_{12}(y) V_1^{(\ell)}(y)^2 \operatorname{sech} y \, dy \right) dx \\ &\quad - \beta_2 \int_{-\infty}^{\infty} V_1^{(\ell)}(x)^4 \, dx, \end{aligned}$$

where

$$\phi_{11}(x) = \frac{1}{2} \operatorname{sech} x (3 - \cosh^2 x - 3x \tanh x), \quad \phi_{12}(x) = \operatorname{sech} x \tanh x.$$

We note that $\phi_{11}(x)$ and $\phi_{12}(x)$ are, respectively, the $(1, 1)$ - and $(1, 2)$ -elements of a fundamental matrix $\Phi(x)$ of the linear system

$$\frac{d}{dx} \begin{pmatrix} \delta U \\ \delta U' \end{pmatrix} = \begin{pmatrix} 0 & 1 \\ \omega - 3U_0(x)^2 & 0 \end{pmatrix} \begin{pmatrix} \delta U \\ \delta U' \end{pmatrix},$$

as which the first equation of the VE (2.1) is rewritten in a first-order system, such that $\Phi(0) = I_2$, where I_n denotes the $n \times n$ identity matrix for $n > 1$. The following result was proven on bifurcations of the fundamental solitary wave (1.5) in Theorem 7.1 of [13] (see also Theorem 5.3 (ii) of [2]).

Theorem 2.1. *For $\ell \in \mathbb{Z}_{\geq 0}$, a pitchfork bifurcation of the fundamental solitary wave (1.5) occurs at $\beta_1 = \beta_1^{(\ell)}$ if $\bar{b}_2 \neq 0$. In addition, it is supercritical or subcritical, depending on whether $\bar{b}_2 > 0$ or < 0 . Moreover, the bifurcated solitary waves are expressed as*

$$(u(t, x), v(t, x)) = (e^{i\omega t} U_\varepsilon(x), e^{ist} V_\varepsilon(x)) \quad (2.3)$$

with

$$U_\varepsilon(x) = U_0(x) + O(\varepsilon^2), \quad V_\varepsilon(x) = \varepsilon V_1^{(\ell)}(x) + O(\varepsilon^3), \quad (2.4)$$

where $\varepsilon > 0$ is a small parameter such that $\beta_1 = \beta_1^{(\ell)} + O(\varepsilon^2)$.

A more precise expression of the bifurcated solitary waves than (2.4) was given in Theorem 7.1 of [13] (see also Theorem 2.2 of [13]). Tractable expressions of the integrals \bar{a}_2 and \bar{b}_2 for computation were also obtained in Proposition 7.4 of [13] (see also Appendix B of [13] for closed-form ones of \bar{b}_2 when $\ell \leq 4$).

We turn to the stability result. The linearized operator of (1.1) around the solitary wave (1.2) with $c, x_0, \theta, \phi = 0$ is given by $J\mathcal{L}$ with

$$J := \begin{pmatrix} O_2 & I_2 \\ -I_2 & O_2 \end{pmatrix}, \quad \mathcal{L} := \begin{pmatrix} \mathcal{L}_+ & O_2 \\ O_2 & \mathcal{L}_- \end{pmatrix}, \quad (2.5)$$

where O_n is the $n \times n$ zero matrix for $n \in \mathbb{N}$ and $n > 1$, and

$$\begin{aligned} \mathcal{L}_+ &:= \begin{pmatrix} -\partial_x^2 + \omega - (3U^2 + \beta_1 V^2) & -2\beta_1 UV \\ -2\beta_1 UV & -\partial_x^2 + s - (\beta_1 U^2 + 3\beta_2 V^2) \end{pmatrix}, \\ \mathcal{L}_- &:= \begin{pmatrix} -\partial_x^2 + \omega - (U^2 + \beta_1 V^2) & 0 \\ 0 & -\partial_x^2 + s - (\beta_1 U^2 + \beta_2 V^2) \end{pmatrix}. \end{aligned} \quad (2.6)$$

See Section 4.2 of [13] for the derivation of the expression of $J\mathcal{L}$ in more general CNLS equations containing (1.1). To discuss the spectral stability of the solitary wave, we consider the associated eigenvalue problem

$$J\mathcal{L}\psi = \lambda\psi, \quad \psi \in L^2(\mathbb{R})^4. \quad (2.7)$$

We easily obtain the following properties of the spectrum $\sigma(J\mathcal{L})$ (see Section 4.1 of [13] for the details):

- (i) If $\lambda \in \sigma(J\mathcal{L})$, then $-\lambda, \pm\bar{\lambda} \in \sigma(J\mathcal{L})$, where the overline represents the complex conjugate. Actually, if $\psi = (\psi_1, \dots, \psi_4)^T$ is an eigenfunction of (2.7) for the eigenvalue λ , then

$$J\mathcal{L}\bar{\psi} = \bar{\lambda}\bar{\psi}, \quad J\mathcal{L} \begin{pmatrix} \psi_1 \\ \psi_2 \\ -\psi_3 \\ -\psi_4 \end{pmatrix} = -\lambda \begin{pmatrix} \psi_1 \\ \psi_2 \\ -\psi_3 \\ -\psi_4 \end{pmatrix}.$$

(ii) The essential spectrum is given by

$$\sigma_{\text{ess}}(J\mathcal{L}) = i(-\infty, -\min\{\omega, s\}] \cup i[\min\{\omega, s\}, \infty). \quad (2.8)$$

(iii) $\text{Ker } J\mathcal{L} = \text{Ker } \mathcal{L}_+ \oplus \text{Ker } \mathcal{L}_-$ contains

$$\begin{aligned} \varphi_1(x) &= (U'(x), V'(x), 0, 0)^T, \\ \varphi_2(x) &= (0, 0, U(x), 0)^T, \quad \varphi_3(x) = (0, 0, 0, V(x))^T. \end{aligned} \quad (2.9)$$

Moreover,

$$\begin{aligned} \chi_1(x) &= (0, 0, -xU(x)/2, -xV(x)/2)^T, \\ \chi_2(x) &= (\partial_\omega U(x), \partial_\omega V(x), 0, 0)^T, \quad \chi_3(x) = (\partial_s U(x), \partial_s V(x), 0, 0)^T \end{aligned} \quad (2.10)$$

satisfy $J\mathcal{L}\chi_j = \varphi_j$, $j = 1, 2, 3$, whenever they exist.

Let $\beta_1 > 0$ and let $\kappa = (-1 + \sqrt{1 + 8\beta_1})/2$. For $(U, V) = (U_0, 0)$ (i.e., the fundamental solitary wave (1.5)), $J\mathcal{L}$ has the eigenvalues

$$\lambda = \pm i(s - \omega(\kappa - k)^2), \quad k \in \{0, 1, \dots, [\kappa]\} \setminus \{\kappa\}, \quad (2.11)$$

and the associated eigenfunctions $\psi = (0, \Psi, 0, \pm i\Psi)^T$ with

$$\Psi(x) = \text{sech}^{\kappa-k}(\sqrt{\omega}x) {}_2F_1\left(\begin{matrix} -k', \kappa - k + k' + 1/2 \\ \kappa - k + 1 \end{matrix}; \text{sech}^2(\sqrt{\omega}x)\right) \quad (2.12)$$

if $k \neq \kappa$ is even ($k = 2k'$, $k' \in \mathbb{Z}_{\geq 0}$), and with

$$\Psi(x) = \text{sech}^{\kappa-k}(\sqrt{\omega}x) \tanh(\sqrt{\omega}x) {}_2F_1\left(\begin{matrix} -k', \kappa - k + k' + 3/2 \\ \kappa - k + 1 \end{matrix}; \text{sech}^2(\sqrt{\omega}x)\right) \quad (2.13)$$

if $k \neq \kappa$ is odd ($k = 2k' + 1$, $k' \in \mathbb{Z}_{\geq 0}$), where the upper or lower signs are taken simultaneously. See Remark 7.6 of [13].

By analyzing the eigenvalue problem (2.7) based on the Evans function technique [1, 8], the following result was proven in Theorem 7.9 of [13].

Theorem 2.2. *The solitary wave (2.3) born at $\beta_1 = \beta_1^{(0)}$ near there as well as the fundamental solitary wave (1.5) for $\beta_1 \in \mathbb{R}$ is spectrally and orbitally stable. The solitary wave (2.3) born at $\beta_1 = \beta_1^{(\ell)}$ with $\ell \geq 1$ is spectrally unstable if*

$$\sqrt{s/\omega} \notin \left\{ -\frac{\ell^2 + k^2}{2(\ell + k)} \mid k \in \{ -\lfloor (\sqrt{2} + 1)\ell \rfloor, \dots, -\ell - 1 \} \right\}. \quad (2.14)$$

Remark 2.3. (i) *If condition (2.14) does not hold, then some purely imaginary eigenvalues of $J\mathcal{L}$ around the fundamental solitary wave are of multiplicity two, so that further tremendous treatments are required to determine their stability.*

(ii) *Pelinovsky and Yang [11] obtained a similar result under some generic conditions which are difficult to actually check for (1.1).*

(iii) *The mechanism of instability for $\ell \geq 1$ is stated as follows. The eigenvalues (2.11) are embedded in the essential spectrum (2.8). Moreover, they have a negative Krein signature if $0 \leq k < \ell$. Since eigenvalues with a negative Krein signature are structurally unstable [5], they split to a pair of eigenvalues with positive and negative real parts under perturbations generically.*

3. COMPUTATIONS OF EIGENVALUES AND EIGENFUNCTIONS

In this section, we give some numerical computation results for eigenvalues and eigenfunctions of the eigenvalue problem (2.7) along with homoclinic solutions to (1.3), and demonstrate the theoretical results stated in Section 2 on bifurcations of the fundamental solitary wave (1.5) and the stability of bifurcated solitary waves in the CNLS equations (1.1) by the numerical ones.

3.1. Numerical Approach. We first briefly describe our numerical approach, which was provided in a general setting in Section 2 of [12].

We begin with computation of homoclinic solutions to (1.3). We slightly modify (1.3), rewrite it in a first-order system as

$$z' = f(z; \beta_1), \quad z = (z_1, z_2, z_3, z_4)^T \in \mathbb{R}^4, \quad (3.1)$$

and numerically compute a homoclinic solution to (3.1) satisfying

$$\lim_{x \rightarrow \pm\infty} z(x) = 0, \quad (3.2)$$

where

$$f(z; \beta_1) := \begin{pmatrix} z_3 \\ z_4 \\ \omega z_1 - (z_1^2 + \beta_1 z_2^2)z_1 + d_1 z_3 \\ s z_2 - (\beta_1 z_1^2 + \beta_2 z_2^2)z_2 + d_1 z_4 \end{pmatrix}$$

with a dummy parameter d_1 . Note that (3.1) is equivalent to (1.3) if $d_1 = 0$. We perform continuation of homoclinic orbits with two parameters since their existence is of codimension one [3]. Moreover, a homoclinic solution persists in (3.1) when one of the other parameters changes only if $d_1 = 0$ (see Lemma 2.13 and Section 5 of [2]).

Let E^s and E^u be, respectively, the two-dimensional stable and unstable subspaces of the linearized system at the origin for (3.1),

$$\delta z' = D_z f(0; \beta_1) \delta z. \quad (3.3)$$

We approximate the homoclinic solution $z(x)$ to (3.1) satisfying (3.2), so that it starts on E^u near the origin at x_- and arrives on E^s near the origin at x_+ , where $x_- < 0 < x_+$ and $|x_{\pm}| \gg 1$. So we look for a solution to (3.1) satisfying

$$L^s z(x_-) = 0, \quad L^u z(x_+) = 0, \quad (3.4)$$

where

$$L^s := \begin{pmatrix} -d_1/2 - \sqrt{\omega + (d_1/2)^2} & 0 & 1 & 0 \\ 0 & -d_1/2 - \sqrt{s + (d_1/2)^2} & 0 & 1 \end{pmatrix}$$

and

$$L^u := \begin{pmatrix} -d_1/2 + \sqrt{\omega + (d_1/2)^2} & 0 & 1 & 0 \\ 0 & -d_1/2 + \sqrt{s + (d_1/2)^2} & 0 & 1 \end{pmatrix}$$

are 2×4 real matrices consisting of row eigenvectors for $D_z f(0; \beta_1)$ such that the associated eigenvalues are negative and positive, respectively. The distances $|z(x_{\pm})|$

should be kept small in the computation. To eliminate the multiplicity of solutions due to the translational symmetry of (1.3), we also add the integral condition

$$\sum_{j=1}^2 \int_{x_-}^{x_+} (z_j(x) - z_j^*(x)) z_{j+2}^*(x) dx = 0, \quad (3.5)$$

where $z^* = (z_1^*, \dots, z_4^*)^T$ represents a previously computed solution along a continuation branch.

We turn to the eigenvalue problem (2.7) and rewrite it as

$$\zeta' = A(x; \beta_1, \lambda) \zeta, \quad \zeta \in \mathbb{C}^8, \lambda \in \mathbb{C}, \quad (3.6)$$

with

$$\lim_{x \rightarrow \pm\infty} \zeta(x) = 0, \quad (3.7)$$

where

$$A(x; \beta_1, \lambda) := \left(\begin{array}{cc|cc} O_4 & & & I_4 \\ \hline A_1(x; \beta_1, \lambda) & \lambda I_2 & & \\ -\lambda I_2 & & A_2(x; \beta_1, \lambda) & \\ \hline & & & O_4 \end{array} \right)$$

with

$$A_1(x; \beta_1, \lambda) := \begin{pmatrix} \omega - (3U^2 + \beta_1 V^2) & -2\beta_1 UV \\ -2\beta_1 UV & s - (\beta_1 U^2 + 3\beta_2 V^2) \end{pmatrix},$$

$$A_2(x; \beta_1, \lambda) := \begin{pmatrix} \omega - (U^2 + \beta_1 V^2) & 0 \\ 0 & s - (\beta_1 U^2 + \beta_2 V^2) \end{pmatrix}.$$

Let $\lambda = \lambda_R + i\lambda_I$ with $\lambda_R, \lambda_I \in \mathbb{R}$ and let

$$A(x; \beta_1, \lambda) = A_R(x; \beta_1, \lambda_R, \lambda_I) + iA_I(x; \beta_1, \lambda_R, \lambda_I),$$

where $A_R(x; \beta_1, \lambda_R, \lambda_I)$ and $A_I(x; \beta_1, \lambda_R, \lambda_I)$ are 8×8 real matrices. Letting $\zeta = \zeta_R + i\zeta_I$ with $\zeta_R, \zeta_I \in \mathbb{R}^8$, we rewrite (3.6) and (3.7) as

$$\begin{aligned} \zeta_R' &= A_R(x; \beta_1, \lambda_R, \lambda_I) \zeta_R - A_I(x; \beta_1, \lambda_R, \lambda_I) \zeta_I, \\ \zeta_I' &= A_I(x; \beta_1, \lambda_R, \lambda_I) \zeta_R + A_R(x; \beta_1, \lambda_R, \lambda_I) \zeta_I \end{aligned} \quad (3.8)$$

and

$$\lim_{x \rightarrow \pm\infty} \zeta_R(x) = \lim_{x \rightarrow \pm\infty} \zeta_I(x) = 0, \quad (3.9)$$

respectively.

Let

$$A_\infty(\beta_1, \lambda) := \lim_{x \rightarrow \pm\infty} A(x; \beta_1, \lambda) = \left(\begin{array}{cccc|cc} O_4 & & & & & I_4 \\ \hline \omega & 0 & \lambda & 0 & & \\ 0 & s & 0 & \lambda & & \\ -\lambda & 0 & \omega & 0 & & \\ 0 & -\lambda & 0 & s & & \\ \hline & & & & & O_4 \end{array} \right)$$

and let \tilde{E}^s and \tilde{E}^u be, respectively, the four-dimensional stable and unstable subspaces of the autonomous linear system

$$\begin{aligned} \zeta_R' &= A_{R\infty}(\beta_1, \lambda_R, \lambda_I) \zeta_R - A_{I\infty}(\beta_1, \lambda_R, \lambda_I) \zeta_I, \\ \zeta_I' &= A_{I\infty}(\beta_1, \lambda_R, \lambda_I) \zeta_R + A_{R\infty}(\beta_1, \lambda_R, \lambda_I) \zeta_I, \end{aligned}$$

where $A_{R\infty}(\beta_1, \lambda_R, \lambda_I)$ and $A_{I\infty}(\beta_1, \lambda_R, \lambda_I)$ are 8×8 real matrices such that

$$A_\infty(\beta_1, \lambda) = A_{R\infty}(\beta_1, \lambda_R, \lambda_I) + iA_{I\infty}(\beta_1, \lambda_R, \lambda_I).$$

Like the homoclinic solution to (3.1), we approximate the solution $(\zeta_R(x), \zeta_I(x))$ to (3.8) satisfying (3.9), so that it starts on \tilde{E}^u near the origin at x_- and arrives on \tilde{E}^s near the origin at x_+ , where x_\pm are the same as in the above. So we look for a solution to (3.8) satisfying

$$\tilde{L}^s \begin{pmatrix} \zeta_R(x_-) \\ \zeta_I(x_-) \end{pmatrix} = 0, \quad \tilde{L}^u \begin{pmatrix} \zeta_R(x_+) \\ \zeta_I(x_+) \end{pmatrix} = 0, \quad (3.10)$$

where

$$\tilde{L}^s := \left(\begin{array}{cc|c|cc|c} -R_+ & -\Delta_+ & I_4 & \Delta_+ & -R_+ & J_4 \\ \Delta_+ & -R_+ & & R_+ & \Delta_+ & \\ \hline -R_- & \Delta_- & I_4 & \Delta_- & R_- & \\ -\Delta_- & -R_- & & -R_- & \Delta_- & -J_4 \end{array} \right),$$

and

$$\tilde{L}^u := \left(\begin{array}{cc|c|cc|c} R_+ & \Delta_+ & I_4 & -\Delta_+ & R_+ & J_4 \\ -\Delta_+ & R_+ & & -R_+ & -\Delta_+ & \\ \hline R_- & -\Delta_- & I_4 & -\Delta_- & -R_- & \\ \Delta_- & R_- & & R_- & -\Delta_- & -J_4 \end{array} \right)$$

with

$$R_\pm := \begin{pmatrix} \rho_{1\pm} & 0 \\ 0 & \rho_{2\pm} \end{pmatrix}, \quad \Delta_\pm := \begin{pmatrix} \delta_{1\pm} & 0 \\ 0 & \delta_{2\pm} \end{pmatrix}, \quad J_4 := \begin{pmatrix} O_2 & I_2 \\ -I_2 & O_2 \end{pmatrix}.$$

Here \tilde{L}^s and \tilde{L}^u are 8×16 real matrices consisting of bases in the subspaces spanned by row eigenvectors for the 16×16 matrix

$$\begin{pmatrix} A_{R\infty}(\lambda_R, \lambda_I) & -A_{I\infty}(\lambda_R, \lambda_I) \\ A_{I\infty}(\lambda_R, \lambda_I) & A_{R\infty}(\lambda_R, \lambda_I) \end{pmatrix}$$

such that the associated eigenvalues have negative and positive real parts, respectively. We have also denoted

$$\sqrt{\omega \pm i\lambda} = \rho_{1\pm} + i\delta_{1\pm}, \quad \sqrt{s \pm i\lambda} = \rho_{2\pm} + i\delta_{2\pm}$$

with

$$\begin{aligned} \rho_{1\pm} &= \sqrt{\frac{\sqrt{(\omega \mp \lambda_I)^2 + \lambda_R^2} + (\omega \mp \lambda_I)}{2}}, \\ \delta_{1\pm} &= \pm \operatorname{sgn}(\lambda_R) \sqrt{\frac{\sqrt{(\omega \mp \lambda_I)^2 + \lambda_R^2} - (\omega \mp \lambda_I)}{2}}, \\ \rho_{2\pm} &= \sqrt{\frac{\sqrt{(s \mp \lambda_I)^2 + \lambda_R^2} + (s \mp \lambda_I)}{2}}, \\ \delta_{2\pm} &= \pm \operatorname{sgn}(\lambda_R) \sqrt{\frac{\sqrt{(s \mp \lambda_I)^2 + \lambda_R^2} - (s \mp \lambda_I)}{2}}. \end{aligned}$$

Unlike $|z(x_\pm)|$, the distances $|\zeta_R(x_\pm)|, |\zeta_I(x_\pm)|$ do not have to be kept small necessarily in the computation since if $(\zeta_R(x_+), \zeta_I(x_+)) \in \tilde{E}^s$ (resp. $(\zeta_R(x_-), \zeta_I(x_-)) \in \tilde{E}^u$) for $|x_\pm| \gg 1$, then $(\zeta_R(x), \zeta_I(x))$ tends to the origin as $x \rightarrow +\infty$ (resp.

TABLE 1. Values of $\beta_1^{(\ell)}$ and \bar{b}_2 for $(\omega, s, \beta_2) = (1, 4, 2)$. The values of \bar{b}_2 are rounded off to the fourth place.

ℓ	0	1	2	3	4
$\beta_1^{(\ell)}$	3	6	10	15	21
\bar{b}_2	5.486	0.3879	0.03650	0.001333	-0.002094

$x \rightarrow -\infty$). To eliminate the multiplicity of solutions due to the linearity of (2.7), we also add the integral conditions

$$\begin{aligned} \sum_{j=1}^4 \int_{x_-}^{x_+} ((\zeta_{Rj}(x) - \zeta_{Rj}^*(x))\zeta_{Rj}^*(x) + (\zeta_{Ij}(x) - \zeta_{Ij}^*(x))\zeta_{Ij}^*(x)) dx &= 0, \\ \sum_{j=1}^4 \int_{x_-}^{x_+} ((\zeta_{Ij}(x) - \zeta_{Ij}^*(x))\zeta_{Rj}^*(x) - (\zeta_{Rj}(x) - \zeta_{Rj}^*(x))\zeta_{Ij}^*(x)) dx &= 0, \end{aligned} \quad (3.11)$$

which are equivalent to

$$\sum_{j=1}^4 \int_{x_-}^{x_+} (\zeta_j(x) - \zeta_j^*(x)) \overline{\zeta_j^*(x)} dx = 0,$$

where $\zeta^* = (\zeta_1^*, \dots, \zeta_8^*)^T$, $\zeta_R^* = (\zeta_{R1}^*, \dots, \zeta_{R8}^*)^T$ and $\zeta_I^* = (\zeta_{I1}^*, \dots, \zeta_{I8}^*)^T$ represent previously computed solutions along continuation branches.

3.2. Numerical Results. We used the computer continuation tool AUTO [4] to obtain numerical solutions to (3.1) and (3.8) satisfying the boundary conditions (3.4) and (3.10), respectively, under the integral conditions (3.5) and (3.11), as in [12]. In the numerical continuations, β_1 was varied along with d_1 , λ_R and λ_I taken as free parameters. Moreover, the homoclinic solution (1.4) and the eigenfunctions (2.12) or (2.13) with the eigenvalues (2.11) were taken as a starting solution. The distances $|z(x_{\pm})|$ were monitored and kept small ($\approx 10^{-3}$ typically).

We set $\omega = 1$, $s = 4$ and $\beta_2 = 2$. The constant \bar{b}_2 appearing in Theorem 2.1 and $\beta_1^{(\ell)}$ were calculated according to the formulas given in Appendix B of [13] and (2.2) as in Table 1. From Theorem 2.1 and Table 1 we see that the first four pitchfork bifurcations are supercritical but the fifth one is subcritical.

Figure 1(a) shows a numerically computed bifurcation diagram of homoclinic solutions to (1.3), which correspond to solitary waves in (1.1), where $x_{\pm} = \pm 7$ were taken except that $x_{\pm} = \pm 5$ for the first branch ($\ell = 0$) because of rapid decaying of the V -component as $x \rightarrow \pm\infty$. We observe that pitchfork bifurcations of solitary waves occur at $\beta_1 = 3, 6, 10, 15, 21$, as predicted in Theorem 2.1 (see also Table 1). Note that a pair of symmetric branches about $V = 0$ are born at each bifurcation point. Moreover, we see that a saddle-node bifurcation of the solitary waves on the fifth branches occurs at $\beta_1 \approx 19.4$ (more precisely, 19.41626...). The homoclinic solutions to (1.3) on the branches born at the first four bifurcation points are displayed for $\beta_1 = 12$ and $\beta_1 = 16$ along with the homoclinic solution (1.4) in Figs. 1(b)-(e). The V -component of the homoclinic orbit on the $(\ell + 1)$ th branch have exactly ℓ zeros for $\ell = 0-4$.

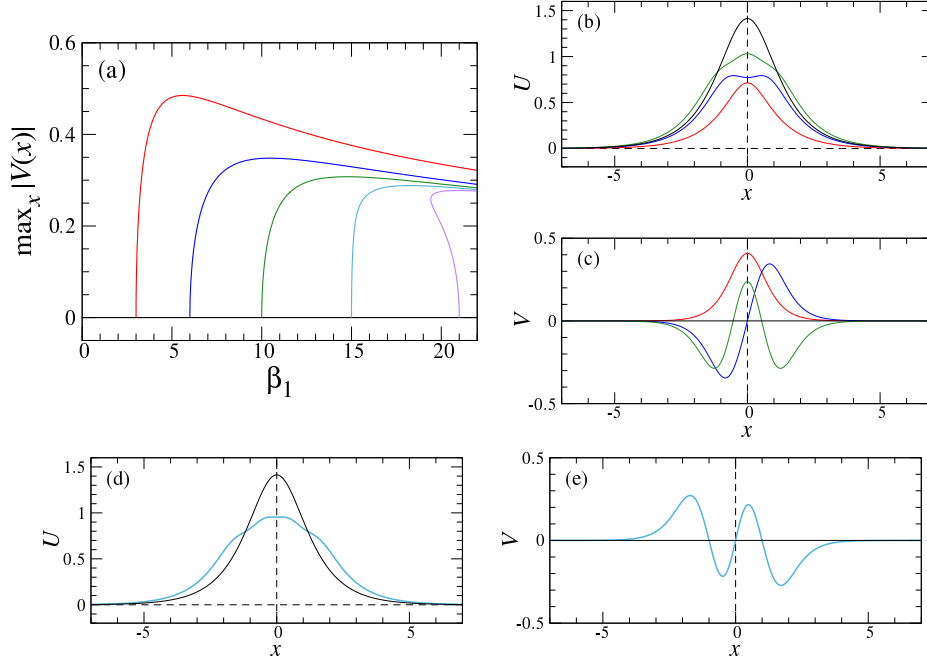


FIGURE 1. Bifurcations of solitary waves in (1.1) for $(\omega, s, \beta_2) = (1, 4, 2)$: (a) Bifurcation diagram; (b) and (c) (resp. (d) and (e)): profiles of the corresponding homoclinic solutions (resp. solution) to (1.3) on the first three branches at $\beta_1 = 12$ (resp. on the fourth branch at $\beta_1 = 16$). In plate (a), the red, blue, green, light blue, and purple lines represent the branches born at the first, second, third, fourth and fifth bifurcations (at $\beta_1 = 3, 6, 10, 15$, and 21), respectively, while the black line represents the branch of the fundamental solitary wave (1.5). In plates (b)-(e), the homoclinic solutions along with (1.4) are plotted as the same color lines as the corresponding branches in plate (a). See Fig. 6 for profiles of the corresponding homoclinic solution to (1.3) on the fifth branch.

The profiles of the bifurcated homoclinic solutions on each branch at $\beta_1 = 50$ and 100 are also plotted with a scaling of $1/\sqrt{\beta_1}$ in Figure 2. Here $x_{\pm} = \pm 8$ were used since some homoclinic solutions do not decay in a long interval (see Figs. 2(d) and (e)). Thus, they converge to certain shapes with a scaling of $1/\sqrt{\beta_1}$ as $\beta_1 \rightarrow \infty$.

Figure 3 shows how the eigenvalues of $J\mathcal{L}$ for the bifurcated solitary wave on each branch change, where $x_{\pm} = \pm 11$ was taken. We only display the eigenvalues with $\text{Re } \lambda, \text{Im } \lambda \geq 0$ since the spectra of $J\mathcal{L}$ are symmetric, as stated in Section 2. For the bifurcated solitary wave born at $\beta_1 = \beta_1^{(\ell)}$, all eigenvalues of $J\mathcal{L}$ at $\beta_1 = \beta_1^{(\ell)}$ are given by

$$\lambda = \pm i(s - \omega(\sqrt{s/\omega} + \ell - k)^2),$$

$$k \in \{0, 1, \dots, \lfloor \sqrt{s/\omega} \rfloor + \ell\} \setminus \{\sqrt{s/\omega} + \ell\}, \quad (3.12)$$

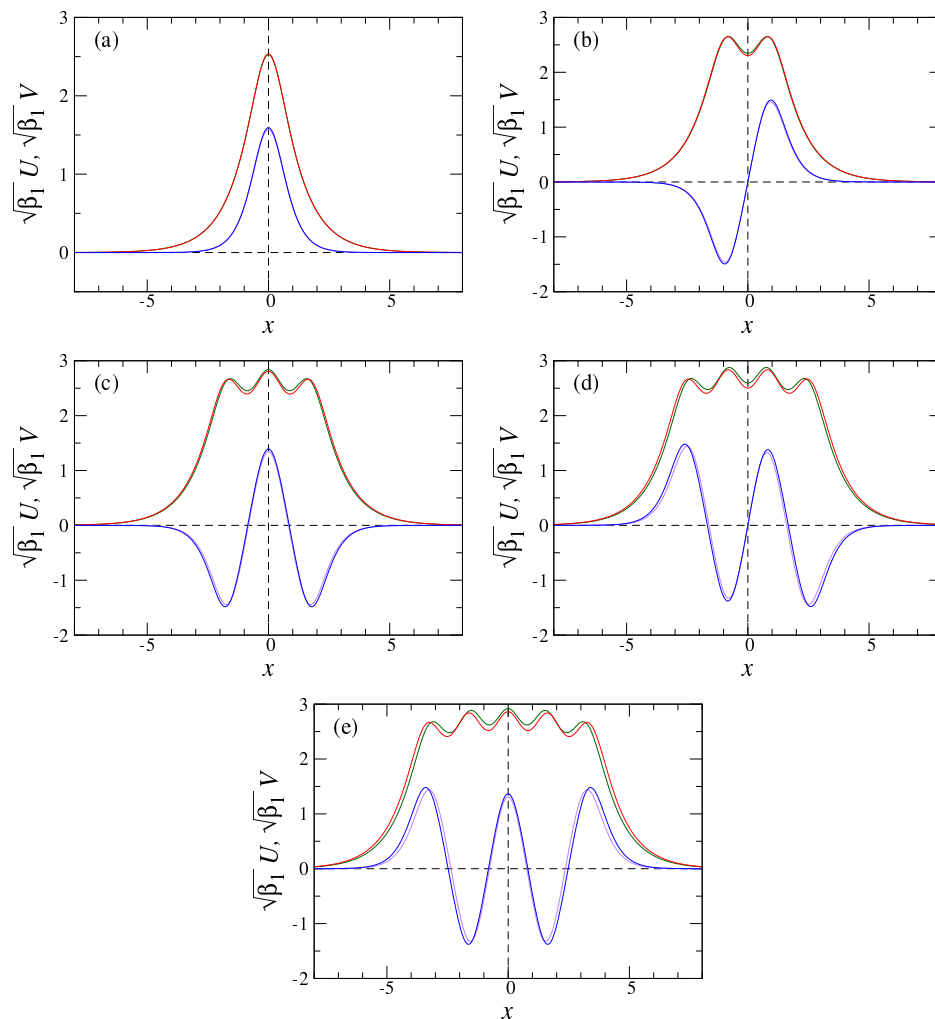


FIGURE 2. Profiles of the homoclinic solutions to (1.3) on each branch at $\beta_1 = 50$ and 100: (a) $\ell = 0$; (b) $\ell = 1$; (c) $\ell = 2$; (d) $\ell = 3$; (e) $\ell = 4$. The red and blue (resp. green and purple) lines, respectively, represents the U - and V -components at $\beta_1 = 100$ (resp. at $\beta_1 = 50$).

(see (2.11)) and they immediately disappear for $k \geq \ell$ when β_1 changes from $\beta_1^{(\ell)}$ (see Remark 7.9 of [13]). The loci of the eigenvalues of $J\mathcal{L}$ leaving the imaginary axis from (3.12) when β_1 changes from $\beta_1^{(\ell)}$ are plotted for $k = 0$ and $\ell = 1$ in Fig. 3(a); for $k = 0, 1$ and $\ell = 2$ in Fig. 3(b); for $k = 0, 1, 2$ and $\ell = 3$ in Fig. 3(c); and $k = 0, 1, 2, 3$ and $\ell = 4$ in Figs. 3(d) and (e). Each curve was computed from $\beta_1 = \beta_1^{(\ell)}$ to 100. Although (3.1) and (3.6) are highly degenerate at the bifurcation point $\beta_1 = \beta_1^{(\ell)}$ since two branches of eigenfunctions are also created there, continuation of their solutions by AUTO succeeded from there. These results

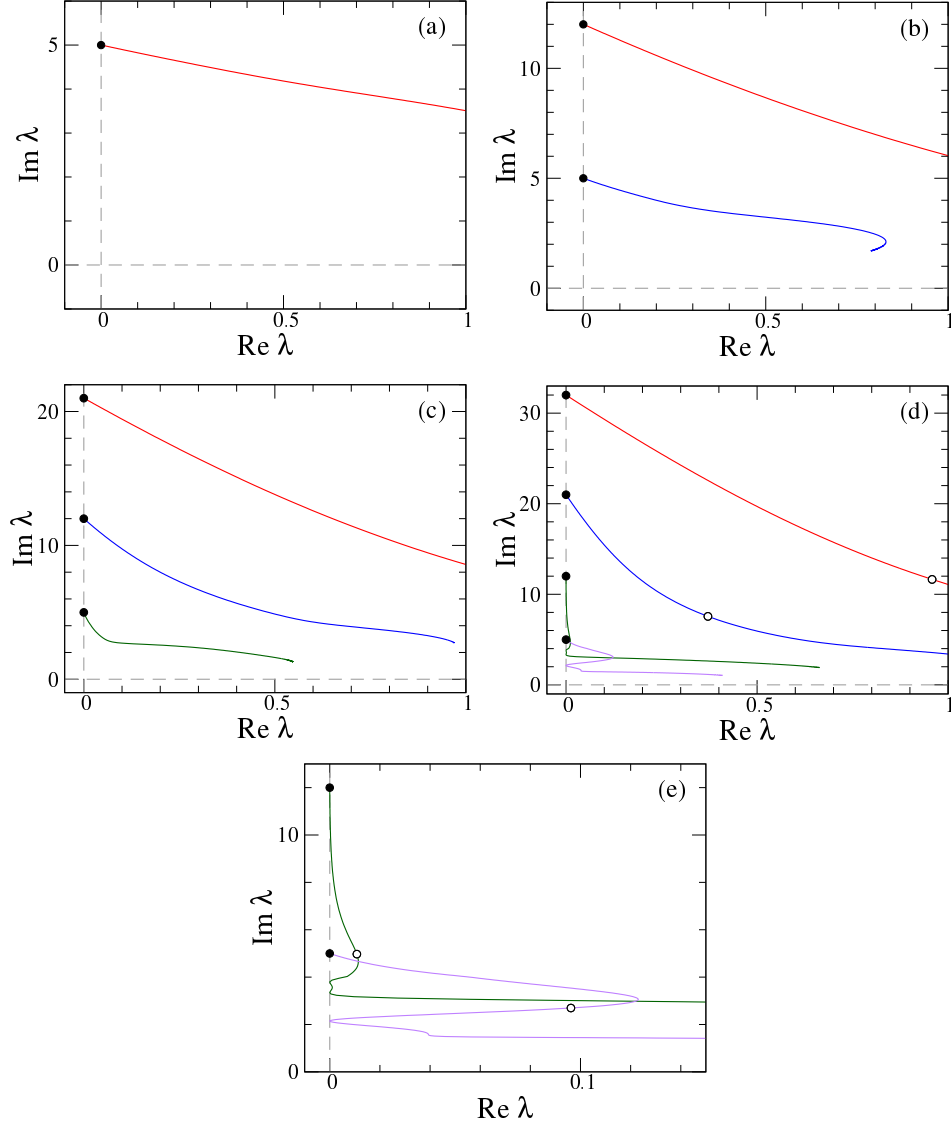


FIGURE 3. Eigenvalues of the linearized operator $J\mathcal{L}$ around the bifurcated solitary wave born at $\beta_1 = \beta_1^{(\ell)}$ for $(\omega, s, \beta_2) = (1, 4, 2)$: (a) $\ell = 1$; (b) $\ell = 2$; (c) $\ell = 3$; (d) and (e) $\ell = 4$. Plate (e) is an enlargement of plate (d). The red, blue, green, and purple lines represent the eigenvalues of $J\mathcal{L}$ with $k = 0, 1, 2$, and 3 , respectively. The bullet ‘•’ represents the loci of the eigenvalues at $\beta_1 = \beta_1^{(\ell)}$. In plates (d) and (e), the circle ‘o’ represents the loci of the eigenvalues at the saddle-node bifurcation point $\beta_1 \approx 19.41626$. Each curve was computed from $\beta_1 = \beta_1^{(\ell)}$ to 100.

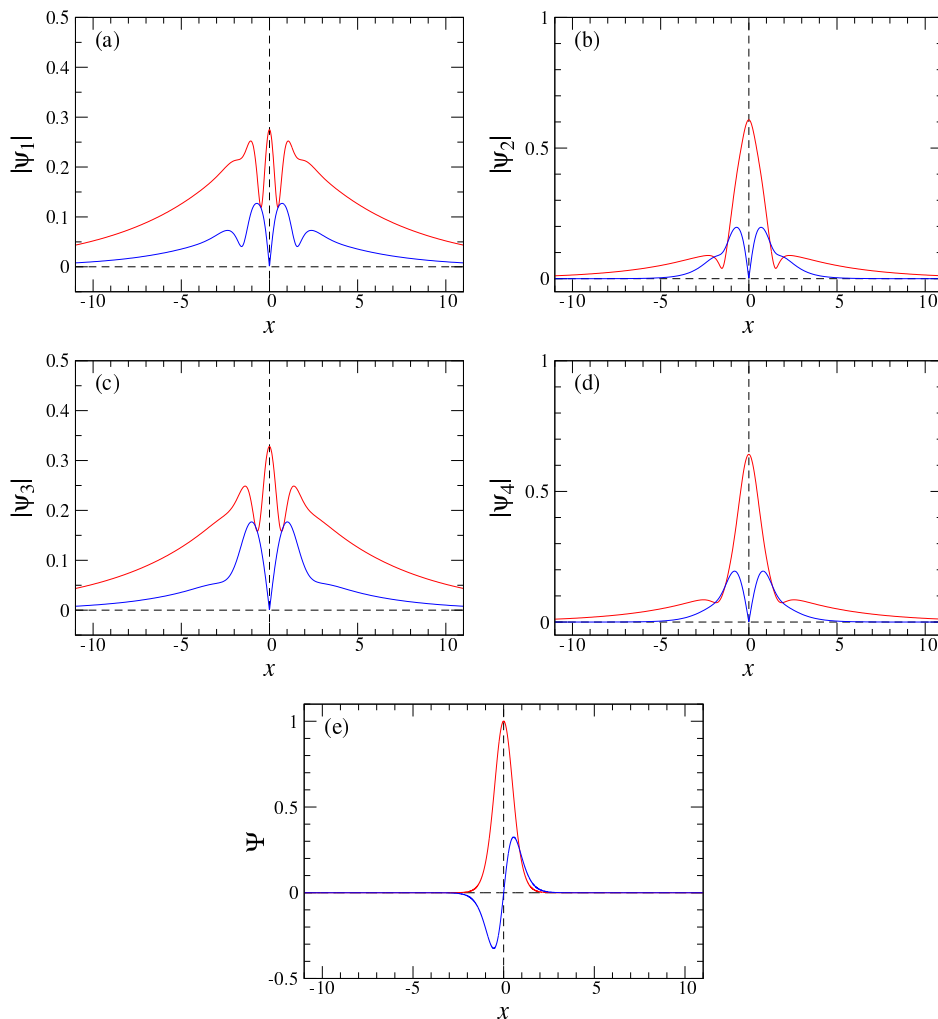


FIGURE 4. Profiles of the eigenfunctions of the eigenvalue problem (2.7) for $\ell = 2$ at $\beta_1 = 12$ with $(\omega, s, \beta_2) = (1, 4, 2)$: (a) $|\psi_1|$; (b) $|\psi_2|$; (c) $|\psi_3|$; (d) $|\psi_4|$; (e) Ψ . The red and blue lines, respectively, represent the eigenfunctions for the curves emerging from 12i and 5i in Fig. 3(b).

indicate that the real parts of the eigenvalues become positive and the bifurcated solitary waves are unstable when $\beta_1 \neq \beta_1^{(\ell)}$, as stated in Theorem 2.2.

On the other hand, the computed eigenvalues at $\beta_1 = 50$ were almost the same as at $\beta_1 = 100$ for all computed branches. So the eigenvalues are thought to converge to certain values as $\beta_1 \rightarrow \infty$. See, e.g., the blue line ($k = 1$) in Fig. 3(b), the blue and green lines ($k = 1$ and 2) in Fig. 3(c), and the green and purple lines ($k = 2$ and 3) in Fig. 3(d). The reason is that as stated above, as $\beta_1 \rightarrow \infty$, the bifurcated homoclinic solutions converge to a certain profile, say $(U_\infty(x), V_\infty(x))$,

with a scaling of $1/\sqrt{\beta_1}$ and the operators \mathcal{L}_\pm in $J\mathcal{L}$ with (2.5) converge to

$$\begin{aligned}\mathcal{L}_+ &= \begin{pmatrix} -\partial_x^2 + \omega - V_\infty^2 & -2U_\infty V_\infty \\ -2U_\infty V_\infty & -\partial_x^2 + s - U_\infty^2 \end{pmatrix}, \\ \mathcal{L}_- &= \begin{pmatrix} -\partial_x^2 + \omega - V_\infty^2 & 0 \\ 0 & -\partial_x^2 + s - U_\infty^2 \end{pmatrix}.\end{aligned}$$

Note that $(U, V) \rightarrow 0$ while $\sqrt{\beta_1}(U, V) \rightarrow (U_\infty, V_\infty)$.

In Figs. 3(d) and (e) four eigenvalues for the bifurcated solitary wave on the fifth branch ($\ell = 4$) are displayed and their values at $\beta_1 = \beta_1^{\text{SN}} \approx 19.41626$, at which a saddle-node bifurcation occurs (see Fig. 1(a)), are plotted as a circle ‘o’. In particular, the solitary wave seems not to change its stability type at the saddle-node bifurcation point since all the eigenvalues are far from the imaginary axis. On the other hand, according to Theorem 2.4 of [2], the VE (2.1) around the corresponding homoclinic solution has two linearly independent solutions there since no bifurcation occurs if it does not, so that the geometrical multiplicity of the zero eigenvalue of $J\mathcal{L}$ increases by one. So we suspect that for the zero eigenvalue a generalized eigenfunction turns to an eigenfunction there, as suggested from Yang’s result [17] for general single NLS equations with external potentials. This suspicion will be numerically proven true in the next section.

Figure 4 displays the absolute value of each component of the corresponding eigenfunction $\psi = (\psi_1, \dots, \psi_4)^T$ for $\ell = 2$ at $\beta_1 = 14$. In Fig. 4(e), the profiles of $\Psi(x)$ for $\ell = 2$, which are given by (2.12) and (2.13) with $k = 0$ and 1, and represent the eigenfunctions associated with the eigenvalues $\lambda = 12i$ and $5i$ there as $\psi = (0, \Psi, 0, i\Psi)^T$, are plotted as the red and blue lines, respectively. We see that the eigenfunctions considerably changes from those at the bifurcation point $\beta_1 = \beta_1^{(2)}$.

4. COMPUTATIONS OF GENERALIZED EIGENFUNCTIONS FOR THE ZERO EIGENVALUES

In this section, for the eigenvalue problem (2.7), we give some numerical computation results for its generalized eigenfunction associated with the zero eigenvalue which turns to an eigenfunction at the saddle-node bifurcation point. These results will demonstrate the correctness of our suspicion stated above on the saddle-node bifurcation observed in Fig. 1(a): the geometric multiplicity of the zero eigenvalue increases by one but the number of eigenvalues counted with their multiplicity on the imaginary axis does not change, so that the solitary wave does not change its stability type at the bifurcation point.

4.1. Numerical Approach. We first recall that φ_j and χ_j , $j = 1, 2, 3$, can be the eigenfunctions and generalized eigenfunctions of (2.7) associated with the zero eigenvalue which are given by (2.9) and (2.10), respectively, such that $J\mathcal{L}\chi_j = \varphi_j$. Moreover, the first and second components of χ_1 are zero while the third and fourth components of χ_2 and χ_3 are zero. Hence, if a generalized eigenfunction χ for the zero eigenvalue becomes an eigenfunction at the saddle-node bifurcation point β_1^{SN} , then χ can be written as a linear combination of χ_2 and χ_3 . This means that the geometric multiplicity is four at $\beta_1 = \beta_1^{\text{SN}}$ but three at $\beta_1 \neq \beta_1^{\text{SN}}$ while the algebraic multiplicity is six for both cases. So we want to compute a generalized

eigenfunction satisfying

$$J\mathcal{L}\psi = \varepsilon_1((1 - \varepsilon_2)\varphi_2 + \varepsilon_2\varphi_3) \quad (4.1)$$

where $\varepsilon_1, \varepsilon_2 \in \mathbb{R}$ are constants. If $\varepsilon_1 = 0$, then ψ becomes an eigenfunction. If $\varepsilon_2 = 0$ and 1 with $\varepsilon_1 = 1$, then $\psi = \chi_2$ and χ_3 , respectively, satisfy (4.1).

Combining (3.1) and (4.1), we write our problem as

$$\begin{pmatrix} z' \\ \eta' \end{pmatrix} = g(z, \eta; \beta_1, \varepsilon_1, \varepsilon_2), \quad z = (z_1, z_2, z_3, z_4)^T, \eta = (\eta_1, \eta_2, \eta_3, \eta_4)^T \in \mathbb{R}^4, \quad (4.2)$$

and numerically compute a homoclinic solution to (4.2) satisfying

$$\lim_{x \rightarrow \pm\infty} z(x) = \lim_{x \rightarrow \pm\infty} \eta(x) = 0, \quad (4.3)$$

where $\eta_j = \psi_j$, $j = 1, 2$, and

$$g(z, \eta; \beta_1, \varepsilon_1, \varepsilon_2) := \begin{pmatrix} z_3 \\ z_4 \\ \omega z_1 - (z_1^2 + \beta_1 z_2^2)z_1 + d_1 z_3 \\ s z_2 - (\beta_1 z_1^2 + \beta_2 z_2^2)z_2 + d_1 z_4 \\ \eta_3 \\ \eta_4 \\ \omega \eta_1 - (3z_1^2 + \beta_1 z_2^2)\eta_1 - 2\beta_1 z_1 z_2 \eta_2 + \varepsilon_1(1 - \varepsilon_2)z_1 + d_2 z_3 \\ s \eta_2 - 2\beta_1 z_1 z_2 \eta_1 - (\beta_1 z_1^2 + 3\beta_2 z_2^2)\eta_2 + \varepsilon_1 \varepsilon_2 z_2 + d_2 z_4 \end{pmatrix}$$

with dummy parameters d_1, d_2 . Here the first and second components of (4.1) and the third and fourth components of ψ have been eliminated since the first and second components of both φ_2 and φ_3 and the third and fourth components of both χ_2 and χ_3 are zero. The fact that the third and fourth components of φ_2 are $(U(x), 0)$ and those of φ_3 are $(0, V(x))$ has also been used (see (2.10)). We easily see that a homoclinic solution persists in (4.2) when one of the other parameters changes only if $d_1 = d_2 = 0$, as in (3.1).

Let \hat{E}^s and \hat{E}^u be, respectively, the four-dimensional stable and unstable subspaces of the linearized system at the origin for (4.2),

$$\begin{pmatrix} \delta z' \\ \delta \eta' \end{pmatrix} = D_{z, \eta} g(0, 0; \beta_1, \varepsilon_1, \varepsilon_2) \begin{pmatrix} \delta z \\ \delta \eta \end{pmatrix}$$

with

$$D_{z, \eta} g(0, 0; \beta_1, \varepsilon_1, \varepsilon_2) = \left(\begin{array}{cccc|cccc} 0 & 0 & 1 & 0 & & & & \\ 0 & 0 & 0 & 1 & & & & \\ \omega & 0 & d_1 & 0 & & & & \\ 0 & s & 0 & d_1 & & & & \\ \hline 0 & 0 & 0 & 0 & 0 & 0 & 1 & 0 \\ 0 & 0 & 0 & 0 & 0 & 0 & 0 & 1 \\ \varepsilon_1(1 - \varepsilon_2) & 0 & d_2 & 0 & \omega & 0 & 0 & 0 \\ 0 & \varepsilon_1 \varepsilon_2 & 0 & d_2 & 0 & s & 0 & 0 \end{array} \right). \quad O_4$$

As in Section 3, we approximate the homoclinic solution $(z(x), \eta(x))^T$ to (4.2) satisfying (4.3), so that it starts on \hat{E}^u near the origin at x_- and arrives on \hat{E}^s near

the origin at x_+ . So we look for a solution to (4.2) satisfying

$$\hat{L}^s \begin{pmatrix} z(x_-) \\ \eta(x_-) \end{pmatrix} = 0, \quad \hat{L}^u \begin{pmatrix} z(x_+) \\ \eta(x_+) \end{pmatrix} = 0, \quad (4.4)$$

where

$$\hat{L}^s := \left(\begin{array}{cc|c} -d_1/2 - \sqrt{\omega + (d_1/2)^2} & 0 & \hat{L}_- \\ 0 & -d_1/2 - \sqrt{s + (d_1/2)^2} & \\ \hat{L}_{31}^s & 0 & \\ 0 & \hat{L}_{42}^s & \end{array} \right),$$

$$\hat{L}^u := \left(\begin{array}{cc|c} -d_1/2 + \sqrt{\omega + (d_1/2)^2} & 0 & \hat{L}_+ \\ 0 & -d_1/2 + \sqrt{s + (d_1/2)^2} & \\ \hat{L}_{31}^u & 0 & \\ 0 & \hat{L}_{42}^u & \end{array} \right)$$

with

$$\begin{aligned} \hat{L}_{31}^s &= \frac{-\varepsilon_1(1-\varepsilon_2) - d_2\sqrt{\omega}}{2\sqrt{\omega}} + \frac{-\varepsilon_1(1-\varepsilon_2) + d_2\sqrt{\omega}}{\sqrt{\omega}} \frac{\sqrt{\omega + (d_1/2)^2} - \sqrt{\omega}}{d_1}, \\ \hat{L}_{42}^s &= \frac{-\varepsilon_1\varepsilon_2 - d_2\sqrt{s}}{2\sqrt{s}} + \frac{-\varepsilon_1\varepsilon_2 + d_2\sqrt{s}}{\sqrt{s}} \frac{\sqrt{s + (d_1/2)^2} - \sqrt{s}}{d_1}, \\ \hat{L}_{31}^u &= \frac{\varepsilon_1(1-\varepsilon_2) - d_2\sqrt{\omega}}{2\sqrt{\omega}} + \frac{\varepsilon_1(1-\varepsilon_2) + d_2\sqrt{\omega}}{\sqrt{\omega}} \frac{\sqrt{\omega + (d_1/2)^2} - \sqrt{\omega}}{d_1}, \\ \hat{L}_{42}^u &= \frac{\varepsilon_1\varepsilon_2 - d_2\sqrt{s}}{2\sqrt{s}} + \frac{\varepsilon_1\varepsilon_2 + d_2\sqrt{s}}{\sqrt{s}} \frac{\sqrt{s + (d_1/2)^2} - \sqrt{s}}{d_1} \end{aligned} \quad (4.5)$$

and

$$\hat{L}_\pm = \begin{pmatrix} 1 & 0 & 0 & 0 & 0 & 0 \\ 0 & 1 & 0 & 0 & 0 & 0 \\ 0 & 0 & \pm\sqrt{\omega} & 0 & 1 & 0 \\ 0 & 0 & 0 & \pm\sqrt{s} & 0 & 1 \end{pmatrix}.$$

Here \hat{L}_+ and \hat{L}_- are 4×8 real matrices consisting of bases in the subspaces spanned by row eigenvectors for $D_{z,\eta}g(0,0;\beta_1,\varepsilon_1,\varepsilon_2)$ such that the associated eigenvalues have negative and positive real parts, respectively. In the computation, the distances $|z(x_\pm)|$ should be kept small but $|\eta(x_\pm)|$ do not have to be small necessarily like $|\zeta_R(x_\pm)|, |\zeta_I(x_\pm)|$ in Section 3.

Furthermore, to monitor the L^2 norm of $(\eta_1, \eta_2)^T$, we add a parameter $c_1 \in \mathbb{R}$ and the integral condition

$$\int_{x_-}^{x_+} (\eta_1(x)^2 + \eta_2(x)^2) dx = c_1. \quad (4.6)$$

From (2.9) we see that if $(z(x), \eta(x))$ is a solution to (4.2) with $d_2 = 0$, then so is $(z(x), \eta(x) + \alpha\eta_0(x))$ for any $\alpha \in \mathbb{R}$, where $\eta_0(x) = (U'(x), V'(x), U''(x), V''(x))$. To monitor the dependence of $\eta(x)$ on $\eta_0(x)$, we add a parameter $c_2 \in \mathbb{R}$ and the integral condition

$$\int_{x_-}^{x_+} (\eta_1(x)z_3(x) + \eta_2(x)z_4(x)) dx = c_2. \quad (4.7)$$

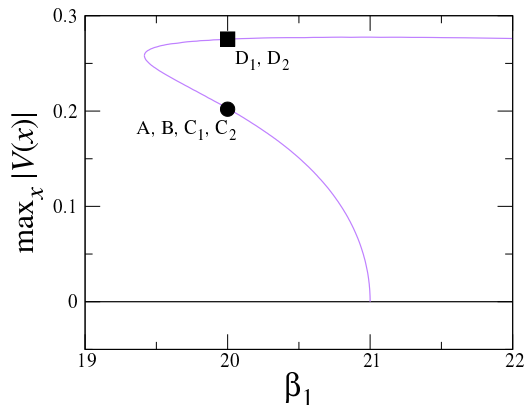


FIGURE 5. Partial enlargement of Fig. 1(a): Bifurcation diagram of solitary waves in (1.1). The labeled solutions in Table 2 are located.

TABLE 2. Summary of the numerical continuations. Here $c_0 \approx 0.074836$ (see (4.9)).

Run no.	Varied parameter	Fixed parameter values				Starting solution	Terminating solution
		β_1	ε_2	c_1	c_2		
1	$c_1 = c_0 \rightarrow 1$	20	0	-	c_0	A	B
2	$c_2 = c_0 \rightarrow 0$	20	0	1	-	B	C_1
3	$\beta_1 = 20 \rightarrow \beta_1^{\text{SN}} \rightarrow 20$	-	0	1	0	C_1	D_1
4	$\varepsilon_2 = 0 \rightarrow 1$	20	-	1	0	C_1	C_2
5	$\beta_1 = 20 \rightarrow \beta_1^{\text{SN}} \rightarrow 20$	-	1	1	0	C_2	D_2

If $c_2 = 0$, then $\eta(x)$ is orthogonal to $\eta_0(x)$. To eliminate the multiplicity of solutions due to the translational symmetry of (1.3), we also add the integral condition (3.5), as in Section 3.1.

4.2. Numerical Results. We set $\omega = 1$, $s = 4$, and $\beta_2 = 2$ as in Section 3.2. Figure 5 is a partial enlargement of Fig. 1(a) in which the pitchfork and saddle-node bifurcation points on the fifth branch are contained. The corresponding homoclinic solutions to (1.3) on the branch are displayed in Fig. 6. We carried out numerical computations stated in Section 4.1 along the branch beyond the saddle-node bifurcation point $\beta_1 = \beta_1^{\text{SN}} \approx 19.41626$. We also used the computer tool AUTO [4] to obtain numerical solutions to (4.2) satisfying the boundary condition (4.4) under the integral conditions (3.5), (4.6), and (4.7), as in Section 3.

Since at the fifth pitchfork bifurcation point $\beta_1 = \beta_1^{(4)} = 21$, $\dim \text{Ker } J\mathcal{L}$ increases by two and consequently (4.2) is highly degenerate, it is difficult to continue a branch of solutions in the boundary value problem beyond there. From this reason we computed the solution branch after the pitchfork bifurcation occurs. As the

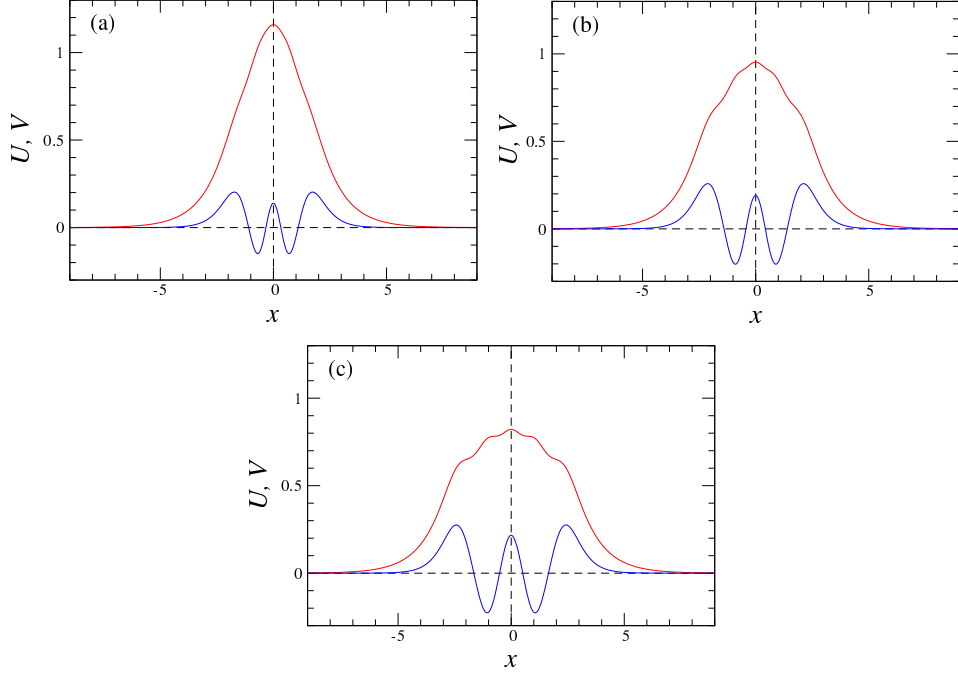


FIGURE 6. Numerically computed homoclinic solutions to (1.3) for $(\omega, s, \beta_2) = (1, 4, 2)$: (a) $\beta_1 = 20$; (b) $\beta_1 = \beta_1^{\text{SN}}$; (c) $\beta_1 = 20$. The red and blue lines, respectively, represents the U - and V -components. The solutions in plates (a) and (c) are, respectively, denoted by \bullet and \blacksquare on the branch in Fig. 5.

starting solution in a series of numerical continuations, we adopted

$$z = (U(x), V(x), U'(x), V'(x))^T \quad \eta = (U'(x), V'(x), U''(x), V''(x))^T \quad (4.8)$$

at $\beta_1 = 20$ on the branch with $\varepsilon_1, \varepsilon_2, d_1, d_2 = 0$, where $U(x), V(x), U'(x)$, and $V'(x)$ were numerically obtained along with

$$\begin{aligned} U''(x) &= \omega U(x) - (U(x)^2 + \beta_1 V(x)^2)U(x), \\ V''(x) &= sV(x) - (\beta_1 U(x)^2 + \beta_2 V(x)^2)V(x) \end{aligned}$$

in advance by another numerical continuation for the boundary value problem of (3.1) with (3.4). We chose $x_{\pm} = \pm 9$ and executed five runs in total. All of the runs are summarized in Table 2. In the numerical continuations, $\beta_1, \varepsilon_2, c_1$ or c_2 was varied while ε_1, d_1 , and d_2 were taken as the free parameters. The distances $|z(x_{\pm})|$ were monitored along with $|\eta(x_{\pm})|$ and kept small ($\approx 10^{-3}$) during the computations. Moreover, since d_1 is very small (it should be zero theoretically), the approximations

$$\frac{\sqrt{\omega + (d_1/2)^2} - \sqrt{\omega}}{d_1} \approx \frac{d_1}{8\sqrt{\omega}}, \quad \frac{\sqrt{s + (d_1/2)^2} - \sqrt{s}}{d_1} \approx \frac{d_1}{8\sqrt{s}},$$

were used in the computations of (4.5).

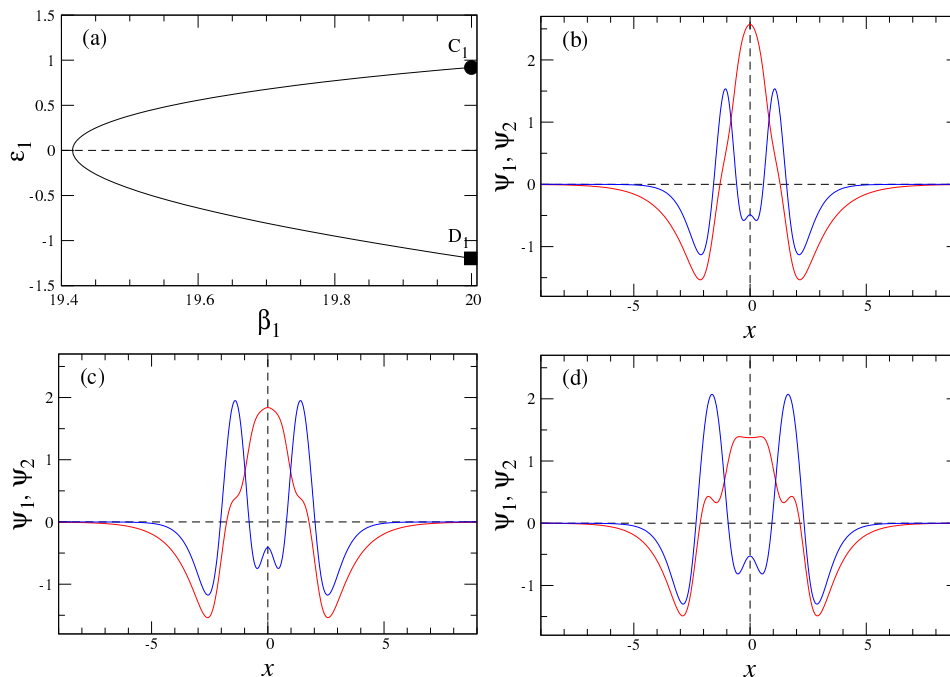


FIGURE 7. Numerically computed generalized eigenfunctions satisfying (4.1) with $\varepsilon_2 = 0$ for $(\omega, s, \beta_2) = (1, 4, 2)$: (a) Solution branch C_1D_1 ; (b) $\beta_1 = 20$ (at C_1); (c) $\beta_1 = \beta_1^{\text{SN}}$; (d) $\beta_1 = 20$ (at D_1). The red and blue lines, respectively, represent the first and second components.

In the first run, we took the numerical solution (4.8) with $(\beta_1, \varepsilon_2) = (20, 0)$ and

$$c_1 = c_2 = \int_{x_-}^{x_+} (U'(x)^2 + V'(x)^2) dx =: c_0 \approx 0.074836 \quad (4.9)$$

labeled by ‘A’ as the starting solution and continued it from $c_1 = c_0$ to 1 for $\beta_1, \varepsilon_2, c_2$ fixed. The solution calculated at $c_1 = 1$, the (η_1, η_2) -components of which are normalized, is labeled by ‘B’. In the second run, we fixed $(\beta_1, \varepsilon_2, c_1) = (20, 0, 1)$ and followed the solution ‘B’ from $c_2 = c_0$ to 0. The solution calculated at $c_2 = 0$, for which $(\eta_1(x), \eta_2(x))$ is orthogonal to $(z_3, z_4) = (U'(x), V'(x))$ by (4.7), is labeled by ‘C₁’. In the third run, we fixed $(\varepsilon_2, c_1, c_2) = (0, 1, 0)$ and followed the solution ‘C₁’ for $J\mathcal{L}\psi = \varepsilon_1\varphi_2$ (see (4.1)) from $\beta_1 = 20$ to β_1^{SN} and from β_1^{SN} to 20. The finally obtained solution is labeled by ‘D₁’. See Fig. 5.

Figure 7 shows generalized eigenfunctions satisfying (4.1) with $\varepsilon_2 = 0$ along with the solution branch obtained from the third run. In particular, at the saddle-node bifurcation point $\beta_1 = \beta_1^{\text{SN}}$, we observe $\varepsilon_1 = 0$, so that the generalized eigenfunction expressed as a linear combination of φ_1 and χ_2 becomes an eigenfunction for the zero eigenvalue in the eigenvalue problem (2.7), as we suspect. Thus, the corresponding solitary wave does not change its stability type at $\beta_1 = \beta_1^{\text{SN}}$: the number of eigenvalues with positive real parts does not change. This is similar to Yang’s result [17] for general single NLS equations with external potentials.

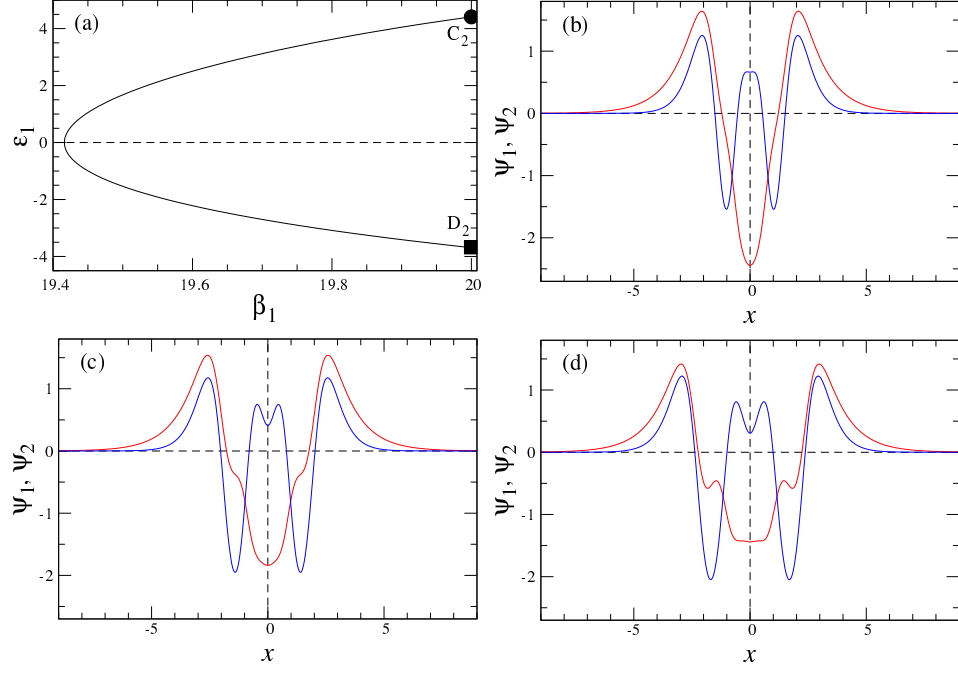


FIGURE 8. Numerically computed generalized eigenfunctions satisfying (4.1) with $\varepsilon_2 = 1$ for $(\omega, s, \beta_2) = (1, 4, 2)$: (a) Solution branch C_2D_2 ; (b) $\beta_1 = 20$ (at C_2); (c) $\beta_1 = \beta_1^{\text{SN}}$; (d) $\beta_1 = 20$ (at D_2). The red and blue lines, respectively, represent the first and second components.

In the fourth run, we fixed $(\beta_1, c_1, c_2) = (20, 1, 0)$ and followed the solution ‘ C_1 ’ from $\varepsilon_2 = 0$ to 1 for $\beta_1 = 20$ fixed. The solution calculated at $\varepsilon_2 = 1$ is labeled by ‘ C_2 ’. In the last run, we fixed $(\varepsilon_2, c_1, c_2) = (1, 1, 0)$ and followed the solution ‘ C_2 ’ for $J\mathcal{L}\psi = \varepsilon_1\varphi_3$ (see (4.1)) from $\beta_1 = 20$ to β_1^{SN} and from β_1^{SN} to 20. The finally obtained solution is labeled by ‘ D_2 ’. See Fig. 5.

Figure 8 shows generalized eigenfunctions satisfying (4.1) with $\varepsilon_2 = 1$ along with the solution branch obtained from the last run. In particular, at the saddle-node bifurcation point $\beta_1 = \beta_1^{\text{SN}}$, we observe $\varepsilon_1 = 0$, so that the generalized eigenfunction expressed as a linear combination of φ_1 and χ_3 becomes an eigenfunction for the zero eigenvalue in the eigenvalue problem (2.7), again. Moreover, the eigenfunction of Fig. 8(c) coincide with that of Fig. 7(c) up to multiplication by -1 . Thus, the generalized eigenfunctions for φ_2 and φ_3 give the same eigenfunction at $\beta_1 = \beta_1^{\text{SN}}$, and $\dim \text{Ker } J\mathcal{L}$ increases by one at $\beta_1 = \beta_1^{\text{SN}}$.

We close this paper with showing that $\dim \text{gKer } J\mathcal{L}$ does not change at β_1^{SN} although the two linearly independent generalized eigenfunctions were observed to converge to the eigenfunction as $\beta_1 \rightarrow \beta_1^{\text{SN}}$.

Fix $\beta_1 = \beta_1^{\text{SN}}$. Let $(\eta_1^{\text{SN}}, \eta_2^{\text{SN}})$ denote the (η_1, η_2) -components of the solution to (4.2) with $(\varepsilon_1, c_2) = (0, 0)$ corresponding to an eigenfunction of (2.7) for the zero eigenvalue, such as plotted in Figs. 7(c) and 8(c). We see that $(\eta_1^{\text{SN}}, \eta_2^{\text{SN}}) \in \text{Ker } \mathcal{L}_+$, where \mathcal{L}_+ is the linear operator given in (2.6). Moreover, $\text{Ker } \mathcal{L}_+$ is of dimension

two at most since the corresponding four-dimensional system of first-order ODEs converges to (3.3) as $x \rightarrow \pm\infty$ and the stable and unstable subspaces of the origin in (3.3) are of dimension two ($\dim E^s = \dim E^u = 2$). So $\{(U', V'), (\eta_1^{\text{SN}}, \eta_2^{\text{SN}})\}$ is a basis of $\text{Ker } \mathcal{L}_+$. Similarly, $\text{Ker } \mathcal{L}_-$ is of dimension two at most and $\{(U, 0), (0, V)\}$ is its basis, where \mathcal{L}_- is the linear operator given in (2.6). Thus, $\text{Ker } J\mathcal{L} = \text{Ker } \mathcal{L}_+ \oplus \text{Ker } \mathcal{L}_-$ is of dimension four and spanned by

$$\{\varphi_1, (\eta_1^{\text{SN}}, \eta_2^{\text{SN}}, 0, 0)^T, \varphi_2, \varphi_3\},$$

where φ_j , $j = 1, 2, 3$, were given in (2.9).

To determine $\text{gKer } J\mathcal{L}$, we consider the solvability of

$$\mathcal{L}_- \begin{pmatrix} \zeta_1 \\ \zeta_2 \end{pmatrix} = \alpha_1 \begin{pmatrix} U' \\ V' \end{pmatrix} + \alpha_2 \begin{pmatrix} \eta_1^{\text{SN}} \\ \eta_2^{\text{SN}} \end{pmatrix} \quad (4.10)$$

and

$$\mathcal{L}_+ \begin{pmatrix} \zeta_1 \\ \zeta_2 \end{pmatrix} = \alpha_1 \begin{pmatrix} U \\ 0 \end{pmatrix} + \alpha_2 \begin{pmatrix} 0 \\ V \end{pmatrix}, \quad (4.11)$$

where α_j , $j = 1, 2$, are constants. Note that nontrivial solutions to (4.10) and (4.11) provide elements of $\text{gKer } J\mathcal{L}$. Numerical integrations carried out in the software AUTO yielded

$$I_1 = \int_{x_-}^{x_+} \eta_1^{\text{SN}}(x)U(x) dx \approx 1.492, \quad I_2 = \int_{x_-}^{x_+} \eta_2^{\text{SN}}(x)V(x) dx \approx -0.373,$$

which indicates along with the Fredholm alternative theorem [7] that there exists an L^2 solution to (4.10) (resp. to (4.11)) if and only if $\alpha_2 = 0$ (resp. $I_1\alpha_1 + I_2\alpha_2 = 0$). Actually, $\zeta = (-xU(x)/2, -xV(x)/2)$ is the solution to (4.10) with $\alpha_2 = 0$, and consequently it is reconfirmed that $\chi_1 \in \text{gKer } J\mathcal{L}$. Thus, there exist two linearly independent generalized eigenfunctions and $\dim \text{gKer } J\mathcal{L}$ does not change at $\beta_1 = \beta_1^{\text{SN}}$.

REFERENCES

- [1] J. Alexander, R. Gardner, and C. Jones, A topological invariant arising in the stability analysis of travelling waves, *J. reine angew. Math.*, **410** (1990) 167–212.
- [2] D. Blázquez-Sanz and K. Yagasaki, Analytic and algebraic conditions for bifurcations of homoclinic orbits I: Saddle equilibria, *J. Differential Equations*, **253** (2012) 2916–2950.
- [3] A. Champneys, Y. Kuznetsov, and B. Sandstede, A numerical toolbox for homoclinic bifurcation analysis, *Int. J. Bifurc. Chaos Appl. Sci. Eng.*, **6** (1996) 867–887.
- [4] E. Doedel and B. Oldeman, AUTO-07P: Continuation and Bifurcation Software for Ordinary Differential Equations, 2012, available online from <http://indy.cs.concordia.ca/auto>.
- [5] M. Grillakis, Analysis of the linearization around a critical point of an infinite dimensional Hamiltonian system, *Commun. Pure Appl. Math.*, **43** (1990) 299–333.
- [6] R. Jackson, On the mechanisms for instability of standing waves in nonlinearly coupled Schrödinger equations, *Nonlinearity*, **24** (2011) 2849–2873.
- [7] T. Kapitula and K. Promislow, *Spectral and Dynamical Stability of Nonlinear Waves*, Springer, New York, 2013.
- [8] Y. Li and K. Promislow, The mechanism of the polarization mode instability in birefringent fiber optics, *SIAM J. Math. Anal.*, **31** (2000) 1351–1373.
- [9] D. Pelinovsky, *Localization in Periodic Potentials: From Schrödinger Operators to the Gross-Pitaevskii Equation*, Cambridge University Press, Cambridge, 2011.
- [10] D. Pelinovsky and J. Yang, Internal oscillations and radiation damping of vector solitons, *Stud. Appl. Math.*, **105** (2000) 245–276.
- [11] D. Pelinovsky and J. Yang, Instabilities of multihump vector solitons in coupled nonlinear Schrödinger equations, *Stud. Appl. Math.*, **115** (2005) 109–137.

- [12] K. Yagasaki and S. Yamazoe, Numerical analyses for spectral stability of solitary waves near bifurcation points, *Jpn J. Ind. Appl. Math.*, **38** (2021) 125–140.
- [13] K. Yagasaki and S. Yamazoe, Bifurcations and spectral stability of solitary waves in coupled nonlinear Schrödinger equations, submitted for publication, arXiv:2005.10317v2.
- [14] J. Yang, Classification of the solitary waves in coupled nonlinear Schrödinger equations, *Physica D*, **108** (1997) 92–112.
- [15] J. Yang, Vector solitons and their internal oscillations in birefringent nonlinear optical fibers, *Stud. Appl. Math.*, **98** (1997) 61–97.
- [16] J. Yang, *Nonlinear Waves in Integrable and Nonintegrable Systems*, SIAM, Philadelphia, PA, 2010.
- [17] J. Yang, No stability switching at saddle-node bifurcations of solitary waves in generalized nonlinear Schrödinger equations, *Phys. Rev. E*, **85** (2012) 037602.

DEPARTMENT OF APPLIED MATHEMATICS AND PHYSICS, GRADUATE SCHOOL OF INFORMATICS,
KYOTO UNIVERSITY, YOSHIDA-HONMACHI, SAKYO-KU, KYOTO 606-8501, JAPAN

Email address: yagasaki@amp.i.kyoto-u.ac.jp (K. Yagasaki)

Email address: yamazoe@amp.i.kyoto-u.ac.jp (S. Yamazoe)